International Journal of Biological Macromolecules 127 (2019) 136–145

Contents lists available at ScienceDirect

International Journal of Biological Macromolecules

journal homepage: http://www.elsevier.com/locate/ijbiomac

Repeated repeat problems: Combinatorial effect of *C9orf72*-derived dipeptide repeat proteins

April L. Darling [a,*], Leonid Breydo [a], Emma G. Rivas [a], Niad T. Gebru [a], Dali Zheng [a], Jeremy D. Baker [a], Laura J. Blair [a], Chad A. Dickey [a], John Koren III [a,*], Vladimir N. Uversky [a,b,*]

[a] Department of Molecular Medicine, College of Medicine, Byrd Alzheimer's Institute, University of South Florida, Tampa, FL 33612, USA
[b] Institute for Biological Instrumentation of the Russian Academy of Sciences, Pushchino, Moscow Region 142290, Russia

ARTICLE INFO

Article history:
Received 4 September 2018
Received in revised form 16 December 2018
Accepted 8 January 2019
Available online 9 January 2019

Keywords:
C9orf72
Dipeptide repeat protein
ALS
FTD
Poly(GA)
Poly(PR)
Intrinsically disordered proteins

ABSTRACT

A microsatellite expansion mutation in *C9orf72* is the most common genetic cause of Amyotrophic Lateral Sclerosis (ALS) and Frontotemporal Dementia (FTD). The expansion mutation leads to *C9orf72* loss of function, RNA foci formation, and generation of five species of non-AUG RAN translated dipeptide repeat proteins (DPRs), such as poly(GA), poly(GP), poly(GR), poly(PA), and poly(PR). Although one cell can contain more than type of DPRs, information about interplay between different DPR species is limited. Here we show that the combined expression of distinct *C9orf72*-derived dipeptide repeat species produces cellular outcomes and structural differences that are unique compared to the expression of a single DPR species, suggesting the complex biological interactions that occur when multiple DPR variants are simultaneously expressed. Our data highlights the need for further analysis of how combined expression of different DPRs affects the disease state.

1. Introduction

A number of neuromuscular and neurodegenerative disorders are classified as microsatellite expansion disorders due to the pathological link to genetic mutations in microsatellite regions. These regions consist of tandem DNA repeats that are prone to strand slippage during replication that leads to the addition or deletion of repetitive segments and a high level of length variation in repeat sequences among individuals [1]. The addition of large repetitive elements in the genome can cause pathology via three separate mechanisms: a loss of function of the expanded gene, production and accumulation of abnormal RNA species that become toxic by sequestering RNA-binding proteins, and a gain of toxic function following the translation of aberrant polypeptide species [2].

Two diseases with pathology driven by microsatellite expansions include amyotrophic lateral sclerosis (ALS) and frontotemporal dementia (FTD). A link connecting these two disorders was discovered when two groups identified a hexanucleotide repeat expansion (HRE) in the 5′ non-coding region of the gene C9 open reading frame 72 (*C9orf72*) gene [3,4]. The discovery of the *C9orf72* expansions has led to the intensive investigation to determine how this genetic aberration promotes disease pathology. Two groups identified aggregation-prone dipeptide repeat (DPR) proteins poly(GA), poly(GP), and poly(GR) in CNS tissue from patients with the *C9orf72* expansion; the products of the sense translation of the expanded microsatellite region [5,6]. Later, it was determined that the antisense sequences can be translated leading to the discovery of poly(PA), poly(PR), and poly(PG) polypeptides [7]. The absence of a start codon indicates these dipeptide species are most likely translated via repeat-associated non-ATG (RAN) translation [7].

Abbreviations: ALS, amyotrophic lateral sclerosis; CD, circular dichroism; CNS, central nervous system; DAPI, 4′,6-diamidino-2-phenylindole; DLS, dynamic light scattering; DMEM, Dulbecco's modified eagle medium; DPR, dipeptide repeat protein; EDTA, ethlenediaminetetraacetic acid; ER, endoplasmic reticulum; FBS, fetal bovine serum; FTD, frontotemporal dementia; HRE, hexanucleotide repeat expansion; IPTG, isopropyl β-D-1-thiogalactopyranoside; ITC, isothermal titration calorimetry; LCD, low complexity domain; PBS, phosphate-buffered saline; PERK, protein kinase R(PKR)-like endoplasmic reticulum kinase; PMSF, phenylmethane sulfonyl fluoride or phenylmethylsulfonyl fluoride; poly(GA), dipeptide repeat protein consisting of glycine-alanine dipeptide repeats; poly(GP), dipeptide repeat protein consisting of glycine-proline dipeptide repeats; poly(GR), dipeptide repeat protein consisting of glycine-arginine dipeptide repeats; poly(PA), dipeptide repeat protein consisting of proline-alanine dipeptide repeats; poly(PR), dipeptide repeat protein consisting of proline-arginine dipeptide repeats; RAN, repeat-associated non-ATG translation; SDS-PAGE, sodium dodecyl sulfate polyacrylamide gel electrophoresis; TBS, Tris-buffered saline; TEM, transmission electron microscopy.

* Corresponding authors at: Department of Molecular Medicine, Morsani College of Medicine, Byrd Alzheimer's Institute, University of South Florida, Tampa, FL 33612, USA.
E-mail addresses: aldarlin@mail.usf.edu (A.L. Darling), jkoren@nd.edu (J. Koren), vuversky@health.usf.edu (V.N. Uversky).

https://doi.org/10.1016/j.ijbiomac.2019.01.035
0141-8130/

Although six DPR species are translated as a result of *C9orf72's* HRE, the biochemical differences between these peptide species produce a diverse set cytotoxic outputs. The arginine-rich polypeptides poly(GR) and poly(PR), which are highly charged, have been shown to be the most toxic species in *Drosophila*, yeast, and mammalian primary neurons [8–12], whereas poly(GA) is able to form toxic amyloid species that can be spread between cells and cause toxicity [13,14]. However, the exact mechanism by which DPRs cause cell death remains unclear. Studies conducted to examine the cellular effects of DPR expression focused on the effects driven by the expression of a single DPR. However, both sense and anti-sense RNA foci from *C9orf72* expansions have been identified in the same cell which suggests that multiple DPRs can be translated simultaneously [15,16]. The phenomena of multiple DPR expression was recently explored in a report which identified poly(GA) as the most abundant DPR expressed in the frontal cortex of patients with expanded *C9orf72* and that poly(GA) could sequester other DPRs [17]. However, additional studies are necessary to more thoroughly evaluate the nature of this sequestration as well as how cells are affected by DPR co-expression.

Here we examined the toxicity produced by individual DPR expression. We identified poly(PR) as the most toxic DPR species in cell models. Since poly(GA) was suggested to be the most prominent DPR species, we then investigated potential interactions between poly(PR) and poly(GA). Interestingly, we demonstrated that expression of poly (GA) can ablate poly(PR)-driven toxicity and reduced markers of ER stress. We then demonstrated that the altered toxicity is likely due to significant structural changes which sequester poly(PR) and poly(GA). Our data illustrates the complex biological interactions that occur when multiple DPR variants are simultaneously expressed and highlights the need for further investigative studies into how DPR expression affects the disease state.

2. Materials and methods

2.1. Cell culture and transfection

NSC34 cells were cultured in Dulbecco's modified eagle medium (DMEM) with 10% FBS and kept at 37 °C with 5% CO_2. NSC34 transfections were performed using Lipofectamine 2000 (Invitrogen, Carlsbad, CA) according to the manufactures instructions, and the media was changed to DMEM containing 5% FBS prior to each transfection. The DPR-containing plasmids used to transfect cells included mCherry-PR_{50}, mCherry-C-1, pEGFP-GA_{50}, pEGFP-GP_{47}, pEGFP-GR_{50}, pEGFP-PA_{50}, pEGFP-PR_{50}, pEGFP-C-1 (Clontech, Mountainview, CA).

2.2. Primary neuron preparation and transfection

All procedures involving the experimentation on animals were done in accordance with the guidelines set forth by the Institutional Animal Care and Use Committee of the University of South Florida. Corticohippocampal neurons were prepared using a previously developed protocol [18]. Briefly, P0 mouse pups were extracted from the womb, their brains were removed, cortices dissected in cold isotonic buffer, washed, digested in trypsin, triturated, and resuspended in DMEM supplemented with 10% FBS and Antibiotic-Antimycotic Solution (Fisher Scientific, Waltham, MA). The cells were then plated on poly-L-lysine (1:5; Sigma, St. Louis, MO) coated coverslips. 24 h after plating, the media was changed to Neurobasal medium (Invitrogen, Carlsbad, CA) supplemented with B27 (Life Technologies, Carlsbad, CA) and Glutamax (Life Technologies, Carlsbad, CA). Neurons were transfected using Lipofectamine LTX (Fisher Scientific, Waltham, MA) according to the manufacturer's instructions. The transfection efficiency for neurons was around 10%, therefore only positively transfected neurons, identified by staining, were used for analysis.

2.3. Antibodies

The following primary antibodies were used in this study: p-PERK (Thr 981) (1:500 Western blot, 1:200 immunofluorescence, Cat. sc-32,577, Santa Cruz, Dallas, TX), PERK (C33E10) (1:1000, Cat, 3192S Cell Signaling, Danvers, MA), Anti-C9ORF72/C9RANT (poly-GA) (1:1000 Western blot, 1:200 immunofluorescence, Cat. MABN889, EMB Millipore, Billerica, MA), Anti-C9ORF72/C9RANT (poly(PR)) (1:1000 Western blot, 1:200 immunofluorescence, Cat. ABN1354, EMB Millipore, Billerica, MA), and Actin (1:1000, Cat. A2066, Sigma, St. Louis, MO). Secondary antibodies used include Alexa-Fluor fluorescently labelled secondary antibodies (1:500, Invitrogen, Carlsbad, CA) and horseradish-peroxidase linked secondary antibodies (1:1000, Southern Biotech, Birmingham, AL).

2.4. Cell staining and imaging

NSC34 cells and primary neurons were prepared for staining 24 or 48 h post-transfection, respectively. Cells were washed with 1× PBS, fixed in 4% paraformaldehyde (w/v) at room temperature for 20 min, and then permeabilized for 10 min with 1× PBS containing 0.1% of Triton X-100. Cells were then blocked with 1× PBS containing 10% goat or donkey serum (Lampire Biological Laboratories Inc. Pipersville, PA). Primary antibody incubations were performed overnight at 4 °C, and secondary antibodies were incubated for 1 h at room temperature. DAPI was added at a concentration of 1:5000 in 1× PBS for 5 min at room temperature. The cover-slips were mounted onto glass slides using Prolong Gold mounting reagent (Life Technologies, Carlsbad, CA). An Olympus FluoView FV10i confocal microscope equipped with a 60× UIS2 SAPO objective was used for imaging. Quantitative analysis was performed using ImageJ software (National Institutes of Health).

2.5. Peptide staining and imaging

0.5 μg of the peptides were added to cover-slips coated with 0.2% electron microscopy grade glutaraldehyde (Electron Microscopy Services, Hatfield, PA) for 2 h at room temperature. They were then washed with 1 × TBS, blocked with 1% BSA in TBS overnight at 4 °C, incubated with the primary antibody for 1 h at room temperature, washed with TBS, and then incubated with the secondary antibody for 1 h at room temperature. The cover-slips were then mounted and slides were imaged as described above.

2.6. Western blotting

Cells were lysed using RIPA protein extraction reagent (50 mM Tris pH 7.4, 150 mM NaCl, 2 mM ethlenediaminetetraacetic acid (EDTA), 1% NP-40, 0.5% sodium dodecyl sulfate) containing 1 mM of PMSF as well as a protease inhibitor mixture (Sigma, St. Louis, MO). 40 μg of the total extracted protein was run on 5–15% gradient SDS-PAGE gels (Bio-Rad, Hercules, CA). The protein was then transferred to a PVDF membrane (Amersham Biosciences, Little Chalfont, United Kingdom), blocked with 7% nonfat milk for 1 h, incubated with the primary antibody overnight at 4 °C, and then incubated with the secondary antibody for 1 h at room temperature. ECL (Fisher Scientific, Waltham, MA) was used to develop blots imaged using a LAS-4000 mini imager (GE Healthcare, Little Chalfont, United Kingdom). ImageJ software (National Institutes of Health) was used to perform densitometry and samples were normalized to the loading control.

2.7. Recombinant protein production and purification

A 50-repeat poly(PR) plasmid was synthesized by Genscript (Piscataway, NJ) in a pet22b vector with a C-terminal GB1 solubility tag. The 50-repeat poly(GA) plasmid was in the pGEX6P.1 vector and was a generous gift from Dr. Leonard Petrucelli (Mayo Clinic,

Jacksonville, FL). *E. coli* BL21 cells were transformed with the plasmids above then grown at 37 °C in LB media containing 100 μg/ml carbenicillin. Once their OD_{600} reached 0.8 the cells were induced with 1 mM of IPTG (Gold Biotechnology, Olivette, MO) for 2 h. Centrifugation at 5000*g* for 15 min was used to harvest the cells, which were then re-suspended with either 1× PBS (GA_{50}) or Nickel chromatography running buffer (20 mM Tris-HCl pH 8.0, 500 mM NaCl, 10 mM Imidazole) (PR_{50}) containing protease inhibitors. The cells were then lysed using a freeze-thaw cycle followed by sonication. The lysed cells were centrifuged at 50,000*g* for 1 h at 4 °C.

The GA_{50} supernatant was affinity purified using a standard gravity column packed with Glutathione Agarose Resin (Fisher Scientific, Waltham, MA), while PR_{50} affinity purification was performed using a HisPur™ Ni-NTA Resin (Fisher Scientific, Waltham, MA). The eluted fractions were dialyzed into 1× PBS overnight and concentrated using an EMD Millipore Amicon™ Ultra-15 Centrifugal Filter Unit (Fisher Scientific, Waltham, MA).

2.8. Peptide synthesis

The GA_{20} and PR_{20} polypeptides were synthesized by DgPeptidesCo., LTD (Hangzhou, China) using the following amino acid sequences:

GA_{20}: GAGAGAGAGAGAGAGAGAGAGAGAGAGAGAGAGAGAG AWDYKDDDDK

PR_{20}: PRPRPRPRPRPRPRPRPRPRPRPRPRPRPRPRPRPRPRWYPYDVPDYA

Aromatic residue (tryptophan) was added at the C-terminal regions of the synthesized peptides to simplify their spectroscopic analyses. Distinct C-terminal tags, FLAG (DYKDDDDK; GA_{20}) and hemagglutinin (YPYDVPDYA; PR_{20}), were added to each DPR.

2.9. Isothermal titration calorimetry (ITC)

Solution of the poly(GA) polypeptide (10 μM) in PBS (10 mM phosphate, 150 mM NaCl, pH 7.5, 1.7 ml) was placed in the sample cell of the VP-ITC calorimeter (Malvern Instruments) and incubated at 25 °C. A solution of the poly(PR) polypeptide (20 μM) in the same buffer was added (19 injections, 15 μl each) and ITC measurements performed. Data was analyzed with Origin software.

2.10. Circular dichroism (CD) spectroscopy

Far-UV CD (190–260 nm) spectra of synthesized polypeptides were measured using a JASCO J-815 spectropolarimeter at 25 °C. A solution of polypeptide (250 μl, 0.1 mg/ml) in the appropriate buffer (10 mM) was incubated for 1 h at 25 °C, placed into a 1 mm pathlength cell, and the CD spectra were acquired with 10 nm/min scan speed at 0.2 nm step size and 1.0 nm bandwidth under constant purging with nitrogen. Two spectra were accumulated and averaged for each sample. Spectra in the presence of 0.15 M NaCl were measured in the 0.2 mm pathlength cell at 0.5 mg/ml protein concentration (60 μl sample volume). Buffers used were citrate (pH 2.0–3.0), acetate (pH 4.0–5.0), phosphate (pH 6.0–7.5), Tris (pH 8.0) and borate (pH 9.0–10.0). The same buffers were used for CD, fluorescence, and DLS measurements.

2.11. Fluorescence spectroscopy

The solution of synthesized polypeptide (13.3 μl, 1 mg/ml stock solution, 5 μg/ml final concentration) was mixed with buffer (final volume 400 μl, final buffer concentration 10 mM). The solution was incubated for 1 h at 25 °C, and the intrinsic protein fluorescence was measured. Excitation wavelength was 280 nm, and emission spectrum was recorded in the 295–380 nm range. Excitation and emission slits were at either 2.5 or 5 nm. The measurements were performed in duplicate for each sample.

2.12. Dynamic light scattering (DLS)

100 μl of the synthesized polypeptide solution (0.1 mg/ml) in the appropriate buffer (10 mM) was placed in the well of the 96-well clear bottom plate (Corning, Corning, NY), and dynamic light scattering was measured. DynaPro plate reader (Wyatt Technology, Goleta, CA) equipped with an 830 nm laser and a temperature control module. Ten 30-s measurements were taken for each well, and the measurements were performed in duplicate. The Dynamics software (Version 7.0.1, Wyatt Technology Corporation) was used for scheduled data acquisition and analysis.

2.13. Nanoparticle tracking analysis

Samples were diluted 500-fold into 1 ml of 0.02 μm filtered deionized water. Approximately 300 μl of sample was loaded onto the Malvern Nanosight LM10 equipped with a 633 nm red laser. Protein particle data were captured with a Marlin CCD camera in duplicate. Graphs were generated by Nanosight software.

2.14. Transmission electron microscopy (TEM)

100 μM of each recombinant GA_{50}, PR_{50}, and GA_{50} + PR_{50} was adsorbed onto prewashed 200 mesh formvar/carbon-coated copper grids for 5 min. The grids were washed with water (10 μl), stained with filtered 2% uranyl acetate (10 μl) for 1 min and washed with water again. The samples were analyzed with a JEOL 1400 Digital Transmission Electron Microscope, and images were captured with a Gatan Orius wide-field camera at the Electron Microscopy Core Facility in the College of Medicine at the University of South Florida.

2.15. Image analysis and statistics

Quantitative analysis was performed using ImageJ software (National Institutes of Health). The statistical significance performed for each analysis was done using ANOVA with Tukey post-tests for group comparison as well as Student's *t*-tests.

3. Results

3.1. Co-expression of poly(PR) with poly(GA) alters the localization, cytotoxic output, and morphology of poly(PR)

We began by characterizing the cytotoxicity of each individual DPR in a cell culture system. Expression of PR_{50} was the most potent reducer of cell viability, though each DPR reduced cell viability relative to the control transfection (Fig. 1A). Since PR_{50} showed the highest toxicity, we examined if the co-expression of the most abundantly expressed DPR, GA_{50}, altered the effects of PR_{50}, similar to the sequestration of other DPRs by poly(GA), as previously reported [17]. To examine this, we expressed GA_{50} alone or in tandem with an increasing amount of PR_{50}. GA_{50} ablated PR_{50} toxicity when expressed at ratios of 10:1 and 5:1 (GA_{50}:PR_{50}) (Fig. 1B). We found this result surprising due to precedent in the literature for poly(GA) presenting cellular toxicities [13,14,17].

Next we wanted to see if the localization of PR_{50} was effected by co-expression with GA_{50} due to poly(PR)'s potential pathological roles in disruption of nuclear transport [8,10,19,20]. We found that PR_{50} alone co-localizes fairly strictly to the nucleus, while co-expression with GA_{50} was able to sequester a large amount of it out of the nucleus and into the cytoplasm (Fig. 1C–D).

Since the co-expression of GA_{50} with PR_{50} rescued PR_{50}-driven cytotoxicity, we examined other poly(PR)-associated cellular stresses in an attempt to identify the cell stress mechanism being ablated by poly (GA) co-expression. Specifically, we were interested in looking at the PERK pathway of the unfolded protein response which can lead to stress

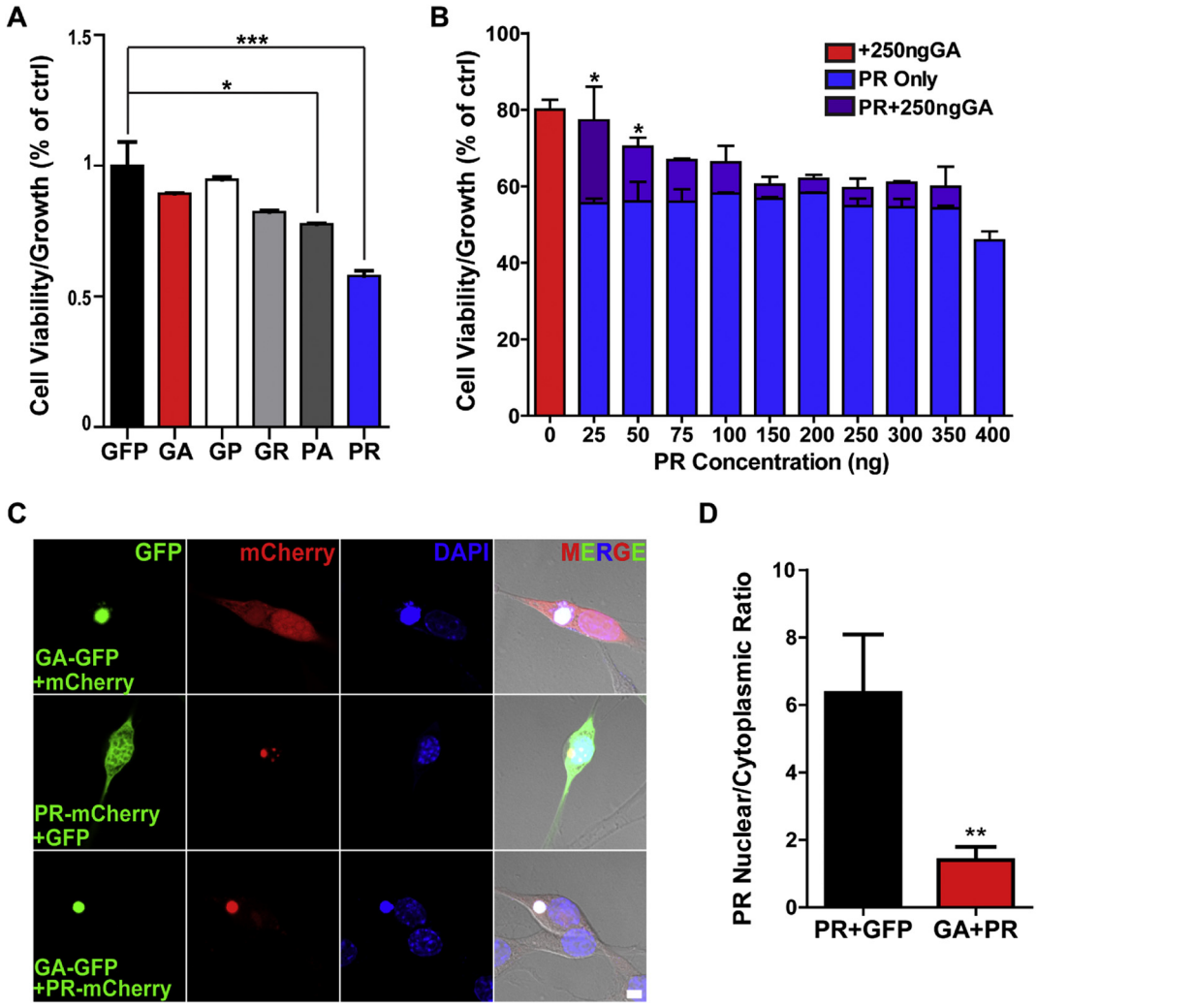

Fig. 1. DPR localization and toxicity (A) NSC34 cells were transfected with 50-repeat GFP-tagged DPR plasmids for 72 h, with Alamar Blue being added for the last 4 h. Absorbance readings taken at 570 nm showed that PR_{50} significantly reduced cell viability and/or cell growth (mean ± SEM, ANOVA with Tukey tests, $^{*}P \le 0.05$, $^{***}P \le 0.001$; n = 3). (B) Co-transfection of varying amount of PR_{50} with 250μg of GA_{50} in the same Alamar Blue assay as that listed above, resulted in a rescue of cell viability and/or growth compared to PR_{50} expression alone at specific ratios (mean ± SEM, ANOVA with Tukey tests, $^{*}P \le 0.05$; n = 3). (C) NSC34 cells were transfected with 50-repeat GFP-tagged GA or 50-repeat mCherry-tagged poy(PR) for 48 h then fixed, stained, and imaged. Scale bar 10 μm. (D) Quantification of the nuclear/cytoplasmic ratio of PR_{50} in the NSC34 cells showed that localization changes to be less nuclear when co-expressed with GA_{50} (mean ± SEM, *t*-test, P = 0.0048; n = 12).

granule formation due to the fact that other disease-related repeat peptides induce cell death in this manner [21]. We found that expression of PR_{50} in HEK293T cells (Fig. 2A & B) and primary neurons (Fig. 2C & D) increased PERK phosphorylation; a cellular event associated with a response to cellular stress, which can trigger apoptosis [22]. The expression of the other DPR species did not lead to any significant differences in the levels of phosphorylated PERK as compared to the control, with the exception of PA_{50}. We then wanted to see if the increase in PERK phosphorylation produced by PR_{50} expression could be altered by co-expression with GA_{50} in primary neurons. We co-transfected primary neurons with GA_{50} and PR_{50}, then immunostained these cells for p-PERK. We found that co-expression of GA_{50} with PR_{50} significantly decreased phosphorylated PERK levels compared to PR_{50} alone, suggesting that GA_{50} was preventing PR_{50} from inducing a fatal ER stress event (Fig. 2C & D).

3.2. Poly(GA) and poly(PR) interact and co-localize in a cell-free environment

We then speculated that the ablation of PR_{50} toxicity was due to DPR sequestration driven by structural changes. To examine this, PR_{50} and GA_{50} were incubated separately or together in the 5:1 ratio observed to reduce PR_{50} toxicity. Using transmission electron microscopy (TEM), we observed that the combination of PR_{50} and GA_{50} presented a morphology distinct from either individual DPR (Fig. 3A).

The observed structural/morphological uniqueness of the PR_{50} and GA_{50} combination prompted us to characterize this interaction further. To more efficiently address structural issues, 20-repeat GA and PR peptides were synthesized (GA_{20} and PR_{20}). A tryptophan residue was added near each C-terminus and distinct C-terminal tags, FLAG (DYKDDDDK; GA_{20}) and hemagglutinin (YPYDVPDYA; PR_{20}), were added to each DPR. We first utilized isothermal titration calorimetry (ITC) to monitor binding of GA_{20} and PR_{20}. After optimization of assay conditions, we found that these polypeptides interacted at ~5:1 poly (GA) to poly(PR) ratio at pH 7.5 in the presence of 150 mM NaCl (Fig. 3B); the same ratio at which GA_{50} negated PR_{50} toxicity in our cellular experiments and at which we observed morphological changes by TEM. The binding between poly(GA) and poly(PR) had a high affinity with a binding constant ~100 nM and was favored both enthalpically and entropically. This binding affinity is similar to that observed for binding of proteins to other highly charged biopolymers, such as heparin [23]. We then performed peptide-immunostaining to confirm

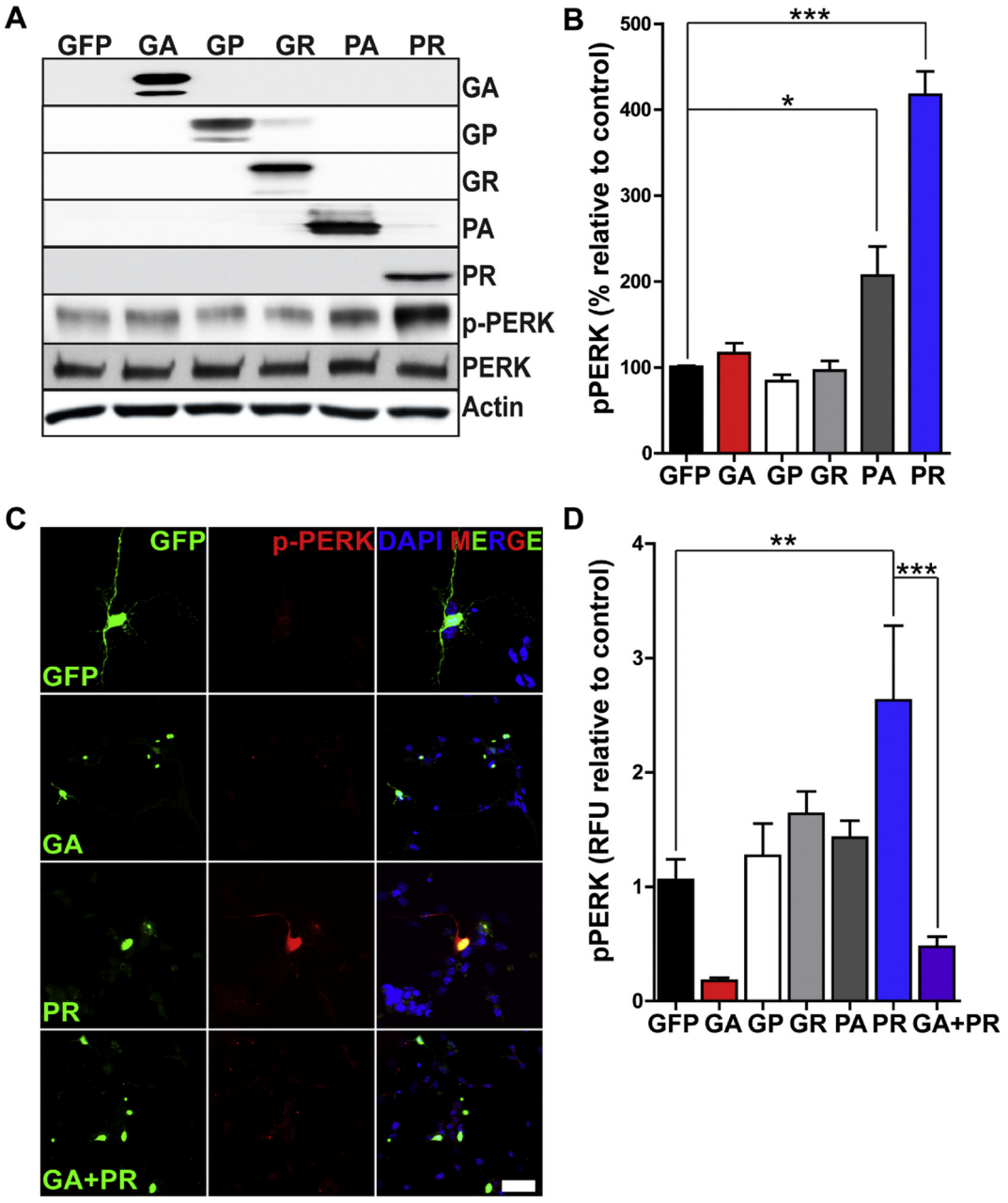

Fig. 2. GA rescues poly(PR) induced increases in pPERK (A) NSC34 cells were transfected with GFP-tagged 50-repeat DPR plasmids for 48 h and the levels of PERK phosphorylation were measured by immunoblotting. (B) Quantitation showed that PR_{50} significantly increases PERK phosphorylation, while the others did not have an effect (mean ± SEM, ANOVA with Tukey tests, $^{*}P \le 0.05$; $^{***}P \le 0.001$; n = 2). (C) Primary murine neurons were transfected with the same plasmids listed above individually and co-transfected with GA_{50} and PR_{50}. They were then immunostained for phosphorylated PERK. Scale bar 10 nm. (D) The quantitative analysis of PERK levels showed PR_{50} significantly increased levels, but this was rescued by co-transfection with GA_{50} (mean ± SEM, ANOVA with Tukey tests, $^{**}P \le 0.01$; $^{***}P \le 0.001$; n = 11).

peptide interaction following co-incubation. Peptide immunostaining demonstrated that the GA_{20} and PR_{20} peptides do co-localize in a cell free environment (Fig. 3C) (Rcoloc = 0.830).

3.3. Co-incubation of poly(PR) with poly(GA) leads to structural changes in synthetic polypeptides

To further characterize the structures formed by the interaction of poly(GA) and poly(PR), we used dynamic light scattering (DLS) to examine the particle sizes of poly(GA), poly(PR), or the combination of poly(GA) and poly(PR). Particle size analysis revealed that co-incubation of GA_{20} and PR_{20} produced particles larger than either individual DPR (Fig. 4A). As a supplement to these DLS results we used nanoparticle tracking analysis to follow protein aggregation by directly observing protein aggregates with light microscopy and tracking their Brownian motion [24]. Similar to our DLS observations, we recorded different populations of aggregates of various sizes for individual polypeptides. However, the nanoparticle tracking analysis of co-incubated GA_{20} and PR_{20} reported that the resulting aggregates were larger in size and occurred at a higher frequency than either individual peptide (Fig. 4B). These results supported the presence of an interaction between GA_{20} and PR_{20} in a cell-free environment.

Next, we examined the secondary structure of these peptides using far-UV circular dichroism (CD) spectroscopy. We measured far-UV CD spectra of GA_{20} and PR_{20} individually and in combination at physiological pH and salt concentrations to determine whether interaction results

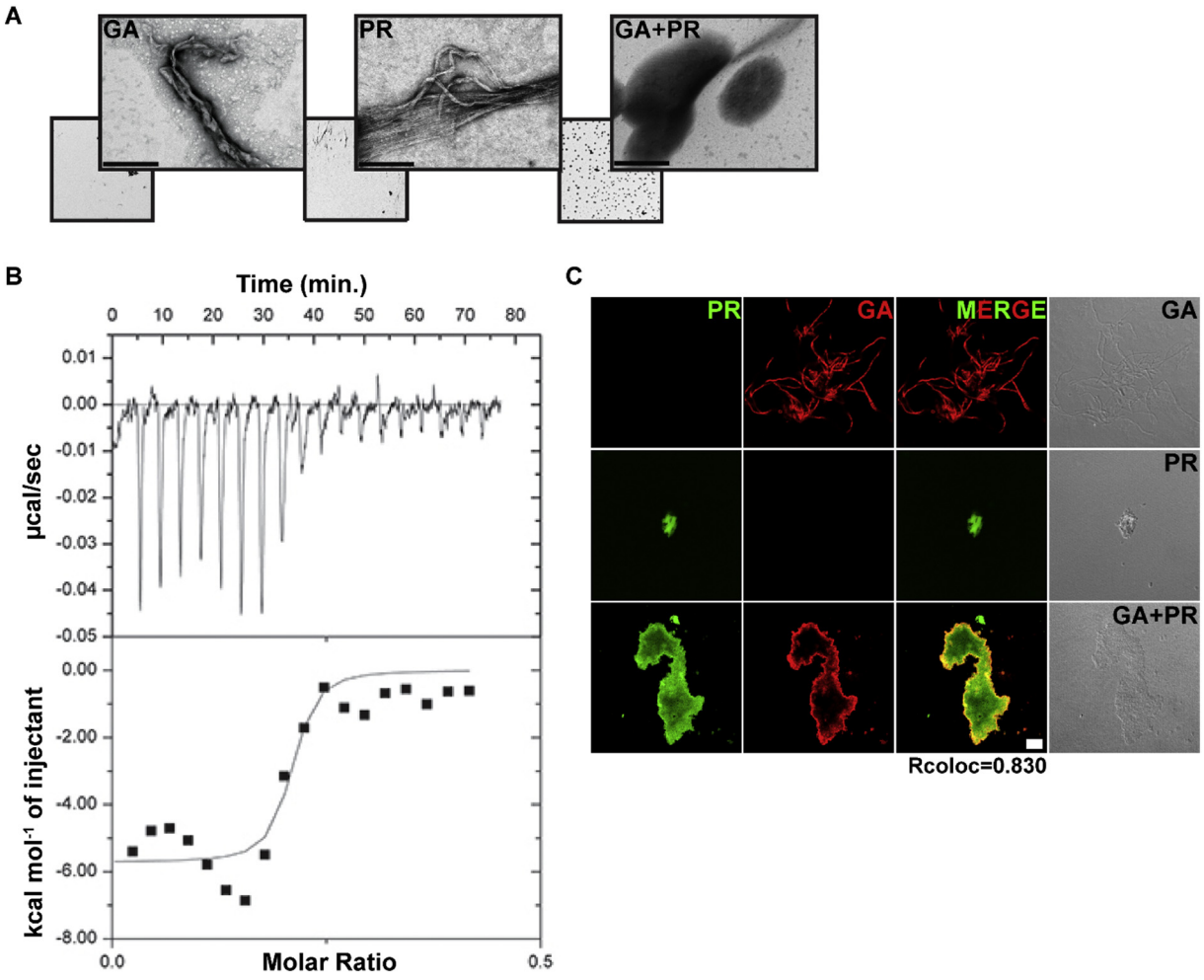

Fig. 3. Poly(GA) and poly(PR) interaction characterization. (A) Transmission electron microscopy was used to visualize recombinant 50-repeat poly(GA), poly(PR), and the combination. Images revealed that upon co-incubation of recombinant GA_{50} with PR_{50} there was a dramatic structural change. Scale bar 100 nm. (B) Isothermal titration calorimetry was utilized to evaluate direct binding of poly(GA) with poly(PR). 10 μM of GA_{20} in PBS was placed in a sample cell of the VP-ITC calorimeter and a 20 μM solution of PR_{20} in PBS was injected (19 injections, 15 μl each) while ITC measurements were performed. After the run was complete the data was analyzed using Origin software. It revealed that the polypeptides interacted at a poly(GA) to poly(PR) ratio of 5:1 in the presence of 150 mM NaCl at pH 7.4. (C) 20-repeat GA-Flag, PR-HA, or a combination were fixed, immunostained with HA and Flag, and imaged. Imaging showed that upon co-incubation the polypeptides are more aggregation prone and colocalize in-vitro (Rcoloc = 0.830). Scale bar 10 μm.

in structural changes. We found that a spectrum of GA_{20} has a minimum at 215–217 nm, which is typical for the proteins with β-sheet rich structures (Fig. 4C). Spectra of poly(PR) contained a minimum at 198–200 nm typical for highly disordered polypeptides (Fig. 4C). Spectra of the mixtures of these polypeptides contained both spectroscopic bands as expected. To determine whether structural changes occurred upon mixing of the polypeptides, the spectra of individual polypeptides were subtracted from the spectrum of their mixture (Fig. 4C; dashed line). The results indicated that there is a loss of β-sheet structure and appearance of disordered structure upon mixing (Fig. 4C), which is an additional indication of interaction between these polypeptides.

We then analyzed the dependence of the GA_{20} and PR_{20} complex on chemical factors such as pH. First, we monitored aggregation of both polypeptides individually and as a mixture by dynamic light scattering over the 2–10 pH range. Dynamic light scattering data showed that GA_{20} is highly aggregation prone at pH 3 while PR_{20} does not aggregate (Fig. 4D; red and blue lines, respectively). Co-incubation of these polypeptides resulted in the shift of the aggregation optimum from pH 3 to physiological pH (pH 6–8) (Fig. 4D; purple line), another indication of direct interaction between the polypeptides. We then examined if secondary structure formation was altered across the same pH range. We recorded the far-UV CD spectra of either the individual polypeptides or the combined GA_{20} and PR_{20} in solutions with a pH range of 2–10. Similar to our observations at physiological pH, we found that the spectrum of GA_{20} has a negative band at 215–217 nm typical for β-sheet-rich structures with minimal alterations occurring across the pH range (Fig. 5A). PR_{20} maintained a minimum around 198–200 nm across pH range (Fig. 5B). The mixture of GA_{20} and PR_{20} demonstrated no structural changes at low pH values (pH 2–4). However, at higher pH values (pH 6–10), we observed a loss of β-sheet structure and the appearance of disordered structure as indicated by characteristic changes in the far-UV CD spectra (Fig. 4E).

An additional measure of protein structure is intrinsic fluorescence of aromatic residues [25]. The addition of tryptophan (Trp) residues near the C-terminus of our synthesized peptides allowed us to examine intrinsic fluorescence as a measure of the hydrophobicity of the polypeptide at different pH values (schematically represented in Fig. 6). We found that the Trp environment in PR_{20} was hydrophilic at all pH values (λ_{em} 349 nm), whereas the Trp environment in GA_{20} was moderately hydrophobic (λ_{em} 339 nm) at pH below 4 and became less hydrophobic (λ_{em} ~343 nm) at higher pH values (Fig. 4F). We generated a calculated fluorescent value for the Trp environment of a mix of poly(GA) and poly(PR) (λ_{em} ~345 nm; Fig. 4F, dashed line). Interestingly, the measured Trp environment from the 1:1 mix of GA_{20} and PR_{20} became steadily more hydrophobic with increasing pH; distinct from the mathematically

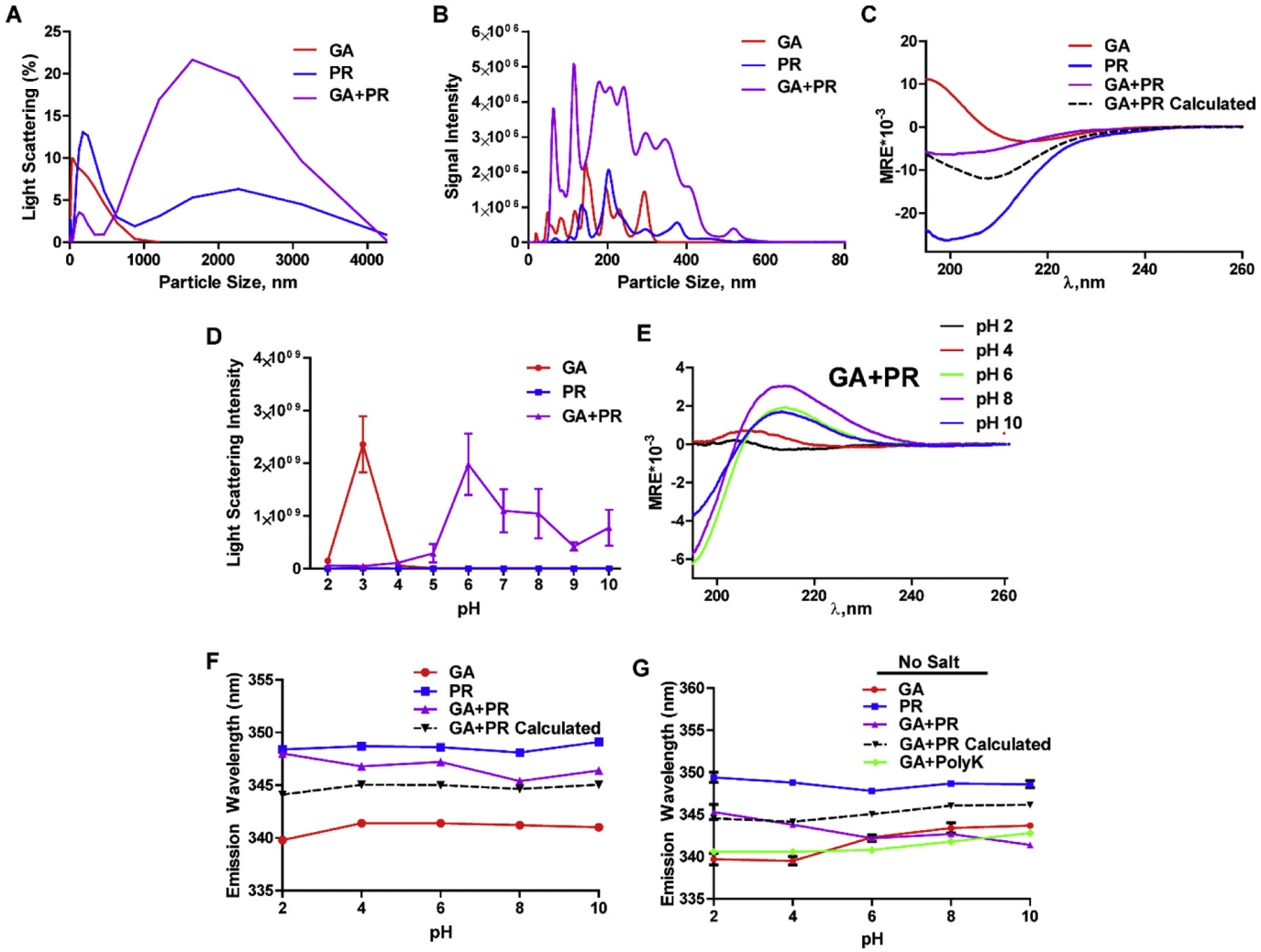

Fig. 4. Physical properties of poly(GA) and poly(PR) interaction (A) Light scattering intensity of GA_{20} and PR_{20} incubated either individually or in combination (0.1 mg/ml) at 25 °C and pH 7.0 in the presence of 0.15 M NaCl. (B) Nanoparticle tracking analysis of GA_{20} and PR_{20} polypeptides incubated either individually (0.1 mg/ml) or in combination at 25 °C and pH 7.5. Red-GA_{20}; blue-PR_{20}; purple-1:1 mixture of GA_{20} and PR_{20}. (C) Far UV CD spectra of GA_{20} (red line), PR_{20} (blue line), and their mixture (purple line) at pH 7.5 in the presence of 0.15 M NaCl. (D) Light scattering intensity of GA_{20} and PR_{20} incubated either individually or in combination (0.1 mg/ml) at 25 °C at different pH values. Red–GA_{20}; blue-PR_{20}; purple-1:1 mixture of GA_{20} and PR_{20}. (E) Far UV CD spectra of combined poly(GA) and pol(PR) peptides at different pH values. (F) Intrinsic fluorescence emission wavelength of GA_{20} and PR_{20} incubated individually or in combination (0.025 mg/ml) at 25 °C at different pH values in the presence of 0.15 M NaCl. Red–GA_{20}; blue-PR_{20}; purple-1:1 mixture of GA_{20} and PR_{20}; black–an average of intrinsic fluorescence emission wavelengths of GA_{20} and PR_{20}. (G) Intrinsic fluorescence emission wavelength of GA_{20} and PR_{20} polypeptides incubated either individually or in combination (0.025 mg/ml) at 25 °C at different pH values. Red–GA_{20}; blue-PR_{20}; purple-1:1 mixture of GA_{20} and PR_{20}; black–an average of intrinsic fluorescence emission wavelengths of GA_{20} and PR_{20}, green–1:1 mixture (by weight) of GA_{20} and poly-K.

averaged λ_{em} values (Fig. 4F). These data suggest the interaction between GA_{20} and PR_{20} produces a distinct secondary or tertiary structure, not observed with either GA_{20} or PR_{20} independently.

We also assessed if the structures formed by GA_{20} and PR_{20} are dependent on physiological salt concentrations. We again monitored the Trp environment in the polypeptides over a 2–10 pH, now in the

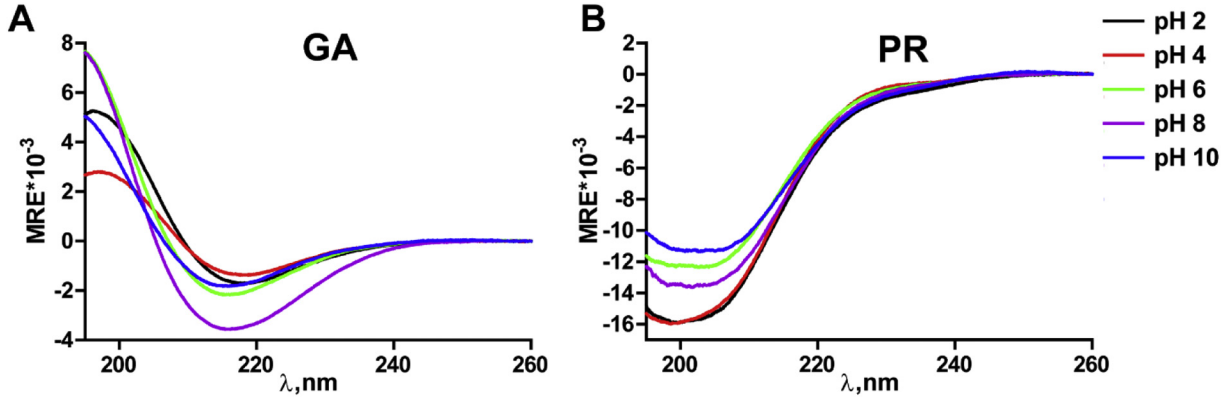

Fig. 5. (A) Far-UV CD spectra of GA_{20} at a 2–10 pH range. (B) Far UV CD spectra of PR_{20} at the same pH range.

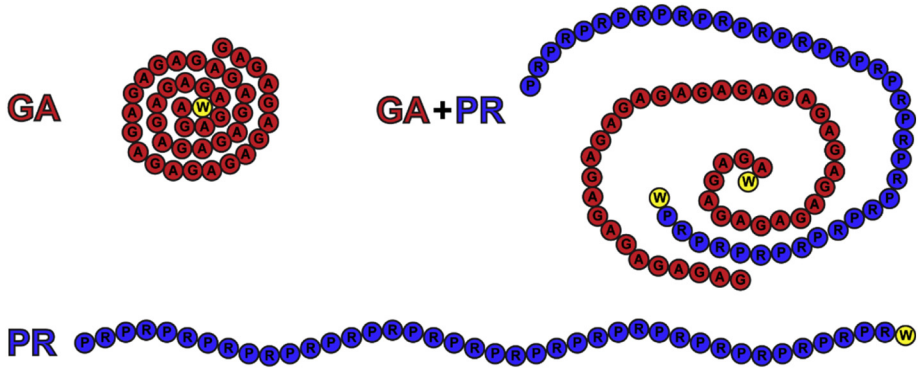

Fig. 6. Schematic of the proposed tryptophan (W) environment in the different conditions. With GA_{20} only the tryptophan is buried in a hydrophobic environment while in PR_{20} only it is freely interacting with the aqueous environment. Upon interaction of the two peptides, the tryptophan in PR_{20} becomes more buried and the environment more hydrophobic.

absence of salt. Similar to conditions with physiological salt concentrations (see: Fig. 4F), we found that PR_{20} was fairly hydrophilic over the pH range (λ_{em} 349 nm). GA_{20} was hydrophobic (λ_{em} 339 nm) below pH 4, but loses hydrophobicity (λ_{em} ~343 nm) at higher pH values (Fig. 4G). We found that the co-incubation of GA_{20} and PR_{20} produced a Trp environment intermediate to those observed in GA_{20} and PR_{20} individually (λ_{em} ~345 nm), and the environment became more hydrophobic when pH values increased (Fig. 4G). We again compared the calculated average of λ_{em} values of each polypeptide and saw that it diverged from the values measured for the GA_{20}-PR_{20} mixture, indicating the formation of a distinct structure when the polypeptides are present at physiological pH values (Fig. 4G).

Since both GA_{20} and PR_{20} contain Trp residues, the extent of contribution of each of these polypeptides to the observed change in Trp environment hydrophobicity is not immediately obvious. To investigate it further and validate our method, we incubated GA_{20} with high molecular weight poly-lysine (poly-K). Though poly-K is not a perfect mimic of PR_{20}, we anticipate the poly-K/GA_{20} interaction to present similarly to GA_{20} and PR_{20} due to the highly positively charged nature and polarity of poly-K. Additionally, poly-K doesn't contain aromatic residues; thus, any changes in the fluorescence emission wavelength are specific to GA_{20}. We observed no significant change in Trp emission wavelength upon addition of poly-K to GA_{20} (Fig. 4G). This indicates that the secondary and tertiary structures adopted by poly(GA) and poly(PR) following incubation are unique to these peptides, and are not a generic structural state which occurs when poly(GA) is present with positively charged peptides. Together, these results suggested that the interaction between GA_{20} and PR_{20} results in the formation of a structure that is unique to the complex between these two DPR species and is dependent on salt and pH conditions.

Since FLAG (DYKDDDDK; GA_{20}) and hemagglutinin (YPYDVPDYA; PR_{20}) tag together with the added reporters in a form of tryptophan residues constitute significant part of the analyzed DPRs, and since these tags contain order-promoting residues (W and Y in GA_{20}-FLAG and W, Y, and V in PR_{20}-hemagglutinin), one might expect that the addition of FLAG and hemagglutinin (HA) tags could affect the structural properties and conformational behavior of poly(GA) and poly(PR) polypeptides analyzed in this study. To partially address these concerns, we conducted computational analysis of the untagged and tagged GA_{20} and PR_{20} DPRs using PONDR® VLXT algorithm [26], which is a commonly used intrinsic disorder predictor with high sensitivity to local peculiarities of protein amino acid sequences [27,28]. Results of this analysis are summarized in Fig. 7, which clearly shows that both DPRs are expected to preserve their mostly disordered nature in the tagged forms. It is clear that this computational analysis is rather superficial, and detailed experimental examination of the effects of different tags on structural properties and conformational behavior of various DPRs is needed. However, despite the general importance of this analysis, it represents an interesting subject of an independent study, which is outside the scopes of this work.

4. Discussion

In this study we identified a unique interaction between poly(GA) and poly(PR) which presents dramatic effects on cell health and stress pathways. Though PR_{50} presented as the most cytotoxic DPR species,

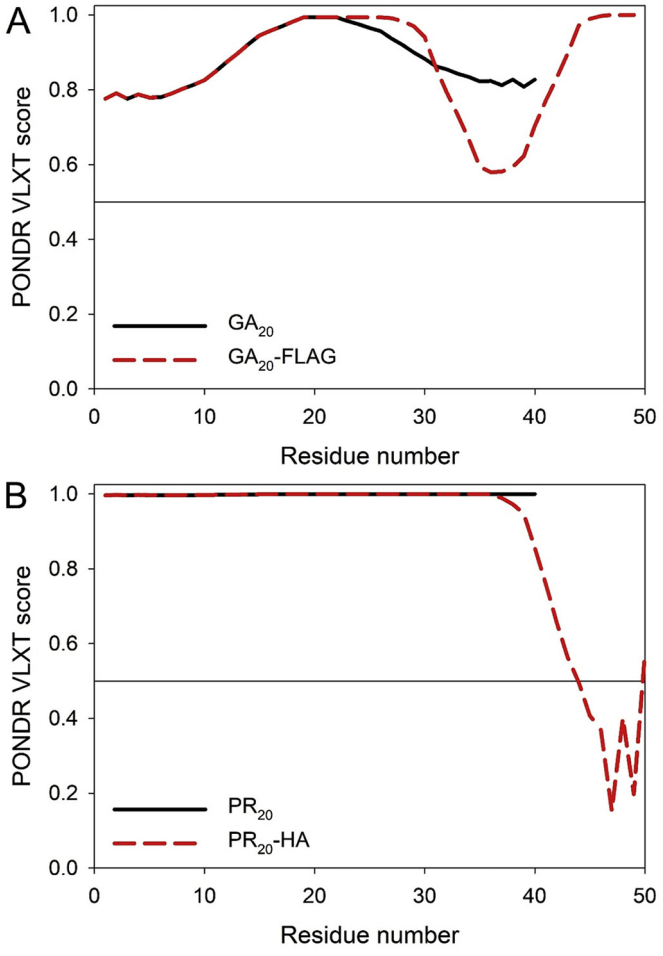

Fig. 7. Analysis of the intrinsic disorder predispositions of the tagged an untagged forms of the GA_{20} (A) and PR_{20} (B). Per-residue disorder propensity was evaluated by PONDR® VLXT algorithm known to be very sensitive to peculiarities of the local disorder predisposition.

co-expression with GA_{50} abrogated this toxicity. An examination of the interaction occurring between recombinant and synthesized poly(PR) and poly(GA) polypeptides demonstrated a clear interaction presenting distinct and discrete structural, biophysical, and morphological properties, as well as an increased aggregation propensity. Taken together, these results indicate that the simultaneous expression of multiple DPR species influence the cytotoxic output of cells in ALS/FTD patients with the C9 expansion mutation. However, it must be taken into account that patients with the expansion mutation often have 1000s of repeats present. Our study, on the other hand, had the limitation of using either 50 or 20 repeats and therefore the results may be altered as compared to looking at disease relevant repeat sizes.

In previous studies it has been shown that poly(PR) has a strong proclivity for interacting with proteins that contain low complexity domains (LCD) [29,30]. Low complexity domains are extremely abundant in eukaryotes and are generally composed of amino acid repeats [31]. The promiscuity of binding exhibited by poly(PR) to LCD-containing proteins has been hypothesized to interfere with several aspects of cellular functioning causing alterations in homeostasis and cytotoxicity [30]. Proteomic analysis of poly(PR) showed that it was able to interact with ALS associated proteins FUS, hnRNPA1, and hnRNPA2B1 [10,29], all of which contain LCDs thought to mediate assembly into higher ordered structures such as liquid droplets [32]. Furthermore, it has been shown that the binding of poly(PR) to LCDs stabilizes these structures [10,29]. Interestingly, ALS associated mutations in these proteins have also been shown to lead to the stability of higher ordered structures and an increase in membrane-less organelles such as stress granules [33–35].

Poly(GA), similar to other ALS pathogenic proteins, can be considered as a low complexity sequence due to its repeated glycine and alanine residues. The chemical nature of the amino acid repeats in poly (GA) is somewhat similar to that contained in the FG repeats in the LCD domain of Nups [36]. Our studies demonstrated that poly(PR) is able to interact with poly(GA). When poly(GA) and poly(PR) interact, there is a morphological change in the peptides that present as spherical liquid-like or highly aggregated higher ordered structures. Since poly (PR) binding to LCDs of ALS related proteins promotes the stabilization of higher ordered structures such as liquid droplets and dense aggregates, it is conceivable that the interaction between poly(PR) and poly (GA) promotes a stabilized higher-order structure that sequesters the toxic poly(PR), and poly(GA), species; preventing the toxicities associated with either individual DPR. These stabilized higher-order structures containing poly(GA) and poly(PR) may have an increased ability to be recognized and cleared by the cell, possibly through autophagy; however, additional studies are necessary to confirm this hypothesis.

Collectively, our results indicate that the specific DPR species being expressed in a cell, as well as the ratio between different species expressed simultaneously, may influence the cytotoxic output of cells in ALS/FTD patients with the *C9* expansion mutation. However, it must be taken into account that the constructs we were experimenting with (20–50 repeats) were much shorter than those present in disease (100–1000s of repeats) and therefore may behave differently. Therefore, further work needs to be done to explore which specific ratios may be exploited to induce or attenuate DPR mediated cytotoxicity and through what mechanism that is occurring by. By elucidating this fact, there will be a clearer pathway for therapeutic developments since the phenomenon of simultaneous DPR expression has been shown to occur in patient tissue.

Author contributions

A.L.D., C.A.D., J.K., and V.N.U. conceived the idea; A.L.D., J.K., and V.N.U. designed the experiments; A.L.D., L.B., E.G.R., D.Z., J.D.B., N.T.G., V.N.U., and L.J.B conducted the experiments; A.L.D., J.K., and V.N.U. wrote the paper.

Declaration of interests

The authors declare no competing interests.

Dedication

This article is dedicated to Dr. Chad A. Dickey, for his inspirational brilliance, creativity and determination.

Acknowledgements

We are thankful to Dr. Leonard Petrucelli (Mayo Clinic, Jacksonville, FL) for the generous gift of the DPR-containing plasmids pEGFP-GA_{50}, pEGFP-GP_{47}, pEGFP-GR_{50}, pEGFP-PA_{50}, and pEGFP-PR_{50} and to Dr. J. Paul Taylor (St. Jude Children's Research Hospital, Memphis, TN) for mCherry-C1 and mCherry-PR_{50} used to transfect cells. We are also thankful to Dr. Bruce Citron (University of South Florida, Tampa, FL) for the generous gift of the NSC34 cell line.

References

[1] J.S. Beckman, J.L. Weber, Survey of human and rat microsatellites, Genomics 12 (4) (1992) 627–631.
[2] M. Goodwin, M.S. Swanson, RNA-binding protein misregulation in microsatellite expansion disorders, Adv. Exp. Med. Biol. 825 (2014) 353–388.
[3] M. DeJesus-Hernandez, I.R. Mackenzie, B.F. Boeve, A.L. Boxer, M. Baker, N.J. Rutherford, A.M. Nicholson, N.A. Finch, H. Flynn, J. Adamson, N. Kouri, A. Wojtas, P. Sengdy, G.Y. Hsiung, A. Karydas, W.W. Seeley, K.A. Josephs, G. Coppola, D.H. Geschwind, Z.K. Wszolek, H. Feldman, D.S. Knopman, R.C. Petersen, B.L. Miller, D.W. Dickson, K.B. Boylan, N.R. Graff-Radford, R. Rademakers, Expanded GGGGCC hexanucleotide repeat in noncoding region of C9ORF72 causes chromosome 9p-linked FTD and ALS, Neuron 72 (2) (2011) 245–256.
[4] A.E. Renton, E. Majounie, A. Waite, J. Simon-Sanchez, S. Rollinson, J.R. Gibbs, J.C. Schymick, H. Laaksovirta, J.C. van Swieten, L. Myllykangas, H. Kalimo, A. Paetau, Y. Abramzon, A.M. Remes, A. Kaganovich, S.W. Scholz, J. Duckworth, J. Ding, D.W. Harmer, D.G. Hernandez, J.O. Johnson, K. Mok, M. Ryten, D. Trabzuni, R.J. Guerreiro, R.W. Orrell, J. Neal, A. Murray, J. Pearson, I.E. Jansen, D. Sondervan, H. Seelaar, D. Blake, K. Young, N. Halliwell, J.B. Callister, G. Toulson, A. Richardson, A. Gerhard, J. Snowden, D. Mann, D. Neary, M.A. Nalls, T. Peuralinna, L. Jansson, V.M. Isoviita, A.L. Kaivorinne, M. Holtta-Vuori, E. Ikonen, R. Sulkava, M. Benatar, J. Wuu, A. Chio, G. Restagno, G. Borghero, M. Sabatelli, D. Heckerman, E. Rogaeva, L. Zinman, J.D. Rothstein, M. Sendtner, C. Drepper, E.E. Eichler, C. Alkan, Z. Abdullaev, S.D. Pack, A. Dutra, E. Pak, J. Hardy, A. Singleton, N.M. Williams, P. Heutink, S. Pickering-Brown, H.R. Morris, P.J. Tienari, B.J. Traynor, A hexanucleotide repeat expansion in C9ORF72 is the cause of chromosome 9p21-linked ALS-FTD, Neuron 72 (2) (2011) 257–268.
[5] P.E. Ash, K.F. Bieniek, T.F. Gendron, T. Caulfield, W.L. Lin, M. Dejesus-Hernandez, M.M. van Blitterswijk, K. Jansen-West, J.W. Paul 3rd, R. Rademakers, K.B. Boylan, D.W. Dickson, L. Petrucelli, Unconventional translation of C9ORF72 GGGGCC expansion generates insoluble polypeptides specific to c9FTD/ALS, Neuron 77 (4) (2013) 639–646.
[6] K. Mori, S.M. Weng, T. Arzberger, S. May, K. Rentzsch, E. Kremmer, B. Schmid, H.A. Kretzschmar, M. Cruts, C. Van Broeckhoven, C. Haass, D. Edbauer, The C9orf72 GGGGCC repeat is translated into aggregating dipeptide-repeat proteins in FTLD/ALS, Science (New York, N.Y.) 339 (6125) (2013) 1335–1338.
[7] T.F. Gendron, K.F. Bieniek, Y.J. Zhang, K. Jansen-West, P.E. Ash, T. Caulfield, L. Daughrity, J.H. Dunmore, M. Castanedes-Casey, J. Chew, D.M. Cosio, M. van Blitterswijk, W.C. Lee, R. Rademakers, K.B. Boylan, D.W. Dickson, L. Petrucelli, Antisense transcripts of the expanded C9ORF72 hexanucleotide repeat form nuclear RNA foci and undergo repeat-associated non-ATG translation in c9FTD/ALS, Acta Neuropathol. 126 (6) (2013) 829–844.
[8] A. Jovicic, J. Mertens, S. Boeynaems, E. Bogaert, N. Chai, S.B. Yamada, J.W. Paul 3rd, S. Sun, J.R. Herdy, G. Bieri, N.J. Kramer, F.H. Gage, L. Van Den Bosch, W. Robberecht, A.D. Gitler, Modifiers of C9orf72 dipeptide repeat toxicity connect nucleocytoplasmic transport defects to FTD/ALS, Nat. Neurosci. 18 (9) (2015) 1226–1229.
[9] S. Mizielinska, S. Gronke, T. Niccoli, C.E. Ridler, E.L. Clayton, A. Devoy, T. Moens, F.E. Norona, I.O.C. Woollacott, J. Pietrzyk, K. Cleverley, A.J. Nicoll, S. Pickering-Brown, J. Dols, M. Cabecinha, O. Hendrich, P. Fratta, E.M.C. Fisher, L. Partridge, A.M. Isaacs, C9orf72 repeat expansions cause neurodegeneration in *Drosophila* through arginine-rich proteins, Science (New York, N.Y.) 345 (6201) (2014) 1192–1194.
[10] K.Y. Shi, E. Mori, Z.F. Nizami, Y. Lin, M. Kato, S. Xiang, L.C. Wu, M. Ding, Y. Yu, J.G. Gall, S.L. McKnight, Toxic PRn poly-dipeptides encoded by the C9orf72 repeat expansion block nuclear import and export, Proc. Natl. Acad. Sci. U. S. A. 114 (7) (2017) E1111–e1117.
[11] H. Tran, S. Almeida, J. Moore, T.F. Gendron, U. Chalasani, Y. Lu, X. Du, J.A. Nickerson, L. Petrucelli, Z. Weng, F.B. Gao, Differential toxicity of nuclear RNA foci versus dipeptide repeat proteins in a *Drosophila* model of C9ORF72 FTD/ALS, Neuron 87 (6) (2015) 1207–1214.
[12] X. Wen, W. Tan, T. Westergard, K. Krishnamurthy, S.S. Markandaiah, Y. Shi, S. Lin, N.A. Shneider, J. Monaghan, U.B. Pandey, P. Pasinelli, J.K. Ichida, D. Trotti, Antisense

proline-arginine RAN dipeptides linked to C9ORF72-ALS/FTD form toxic nuclear aggregates that initiate in vitro and in vivo neuronal death, Neuron 84 (6) (2014) 1213–1225.
[13] Y.J. Chang, U.S. Jeng, Y.L. Chiang, I.S. Hwang, Y.R. Chen, The glycine-alanine dipeptide repeat from C9orf72 hexanucleotide expansions forms toxic amyloids possessing cell-to-cell transmission properties, J. Biol. Chem. 291 (10) (2016) 4903–4911.
[14] S. May, D. Hornburg, M.H. Schludi, T. Arzberger, K. Rentzsch, B.M. Schwenk, F.A. Grasser, K. Mori, E. Kremmer, J. Banzhaf-Strathmann, M. Mann, F. Meissner, D. Edbauer, C9orf72 FTLD/ALS-associated Gly-Ala dipeptide repeat proteins cause neuronal toxicity and Unc119 sequestration, Acta Neuropathol. 128 (4) (2014) 485–503.
[15] S. Mizielinska, T. Lashley, F.E. Norona, E.L. Clayton, C.E. Ridler, P. Fratta, A.M. Isaacs, C9orf72 frontotemporal lobar degeneration is characterised by frequent neuronal sense and antisense RNA foci, Acta Neuropathol. 126 (6) (2013) 845–857.
[16] M. Yamakawa, D. Ito, T. Honda, K. Kubo, M. Noda, K. Nakajima, N. Suzuki, Characterization of the dipeptide repeat protein in the molecular pathogenesis of c9FTD/ALS, Hum. Mol. Genet. 24 (6) (2015) 1630–1645.
[17] Y.B. Lee, P. Baskaran, J. Gomez, H.J. Chen, A. Nishimura, B. Smith, C. Troakes, Y. Adachi, A. Stepto, L. Petrucelli, J.M. Gallo, F. Hirth, B. Rogelj, S. Guthrie, C.E. Shaw, C9orf72 poly GA RAN-translated protein plays a key role in amyotrophic lateral sclerosis via aggregation and toxicity, Hum. Mol. Genet. 26 (24) (2017) 4765–4777.
[18] C. Katnik, W.R. Guerrero, K.R. Pennypacker, Y. Herrera, J. Cuevas, Sigma-1 receptor activation prevents intracellular calcium dysregulation in cortical neurons during in vitro ischemia, J. Pharmacol. Exp. Ther. 319 (3) (2006) 1355–1365.
[19] B.D. Freibaum, Y. Lu, R. Lopez-Gonzalez, N.C. Kim, S. Almeida, K.H. Lee, N. Badders, M. Valentine, B.L. Miller, P.C. Wong, L. Petrucelli, H.J. Kim, F.B. Gao, J.P. Taylor, GGGGCC repeat expansion in C9orf72 compromises nucleocytoplasmic transport, Nature 525 (7567) (2015) 129–133.
[20] K. Zhang, C.J. Donnelly, A.R. Haeusler, J.C. Grima, J.B. Machamer, P. Steinwald, E.L. Daley, S.J. Miller, K.M. Cunningham, S. Vidensky, S. Gupta, M.A. Thomas, I. Hong, S.L. Chiu, R.L. Huganir, L.W. Ostrow, M.J. Matunis, J. Wang, R. Sattler, T.E. Lloyd, J.D. Rothstein, The C9orf72 repeat expansion disrupts nucleocytoplasmic transport, Nature 525 (7567) (2015) 56–61.
[21] Y. Kouroku, E. Fujita, I. Tanida, T. Ueno, A. Isoai, H. Kumagai, S. Ogawa, R.J. Kaufman, E. Kominami, T. Momoi, ER stress (PERK/eIF2alpha phosphorylation) mediates the polyglutamine-induced LC3 conversion, an essential step for autophagy formation, Cell Death Differ. 14 (2) (2007) 230–239.
[22] M. Marton, A. Kurucz, B. Lizak, E. Margittai, G. Banhegyi, O. Kapuy, A systems biological view of life-and-death decision with respect to endoplasmic reticulum stress-the role of PERK pathway, Int. J. Mol. Sci. 18 (1) (2017).
[23] A.K. Dutta, J. Rosgen, K. Rajarathnam, Using isothermal titration calorimetry to determine thermodynamic parameters of protein-glycosaminoglycan interactions, Methods Mol. Biol. 1229 (2015) 315–324.
[24] W. Tatkiewicz, E. Elizondo, E. Moreno, C. Diez-Gil, N. Ventosa, J. Veciana, I. Ratera, Methods for characterization of protein aggregates, Methods Mol. Biol. 1258 (2015) 387–401.
[25] V. I. Razinkov, M. J. Treuheit, G. W. Becker, Methods of high throughput biophysical characterization in biopharmaceutical development, Curr. Drug Discov. Technol. 10 (1) (2013) 59–70.
[26] P. Romero, Z. Obradovic, X. Li, E.C. Garner, C.J. Brown, A.K. Dunker, Sequence complexity of disordered protein, Proteins 42 (1) (2001) 38–48.
[27] Y. Cheng, C.J. Oldfield, J. Meng, P. Romero, V.N. Uversky, A.K. Dunker, Mining alpha-helix-forming molecular recognition features with cross species sequence alignments, Biochemistry 46 (47) (2007) 13468–13477.
[28] C.J. Oldfield, Y. Cheng, M.S. Cortese, P. Romero, V.N. Uversky, A.K. Dunker, Coupled folding and binding with alpha-helix-forming molecular recognition elements, Biochemistry 44 (37) (2005) 12454–12470.
[29] K.H. Lee, P. Zhang, H.J. Kim, D.M. Mitrea, M. Sarkar, B.D. Freibaum, J. Cika, M. Coughlin, J. Messing, A. Molliex, B.A. Maxwell, N.C. Kim, J. Temirov, J. Moore, R.M. Kolaitis, T.I. Shaw, B. Bai, J. Peng, R.W. Kriwacki, J.P. Taylor, C9orf72 dipeptide repeats impair the assembly, dynamics, and function of membrane-less organelles, Cell 167 (3) (2016) 774–788.e17.
[30] Y. Lin, E. Mori, M. Kato, S. Xiang, L. Wu, I. Kwon, S.L. McKnight, Toxic PR polydipeptides encoded by the C9orf72 repeat expansion target LC domain polymers, Cell 167 (3) (2016) 789–802.e12.
[31] M. Toll-Riera, N. Rado-Trilla, F. Martys, M.M. Alba, Role of low-complexity sequences in the formation of novel protein coding sequences, Mol. Biol. Evol. 29 (3) (2012) 883–886.
[32] M. Kato, T.W. Han, S. Xie, K. Shi, X. Du, L.C. Wu, H. Mirzaei, E.J. Goldsmith, J. Longgood, J. Pei, N.V. Grishin, D.E. Frantz, J.W. Schneider, S. Chen, L. Li, M.R. Sawaya, D. Eisenberg, R. Tycko, S.L. McKnight, Cell-free formation of RNA granules: low complexity sequence domains form dynamic fibers within hydrogels, Cell 149 (4) (2012) 753–767.
[33] A. Molliex, J. Temirov, J. Lee, M. Coughlin, A.P. Kanagaraj, H.J. Kim, T. Mittag, J.P. Taylor, Phase separation by low complexity domains promotes stress granule assembly and drives pathological fibrillization, Cell 163 (1) (2015) 123–133.
[34] T. Murakami, S. Qamar, J.Q. Lin, G.S. Schierle, E. Rees, A. Miyashita, A.R. Costa, R.B. Dodd, F.T. Chan, C.H. Michel, D. Kronenberg-Versteeg, Y. Li, S.P. Yang, Y. Wakutani, W. Meadows, R.R. Ferry, L. Dong, G.G. Tartaglia, G. Favrin, W.L. Lin, D.W. Dickson, M. Zhen, D. Ron, G. Schmitt-Ulms, P.E. Fraser, N.A. Shneider, C. Holt, M. Vendruscolo, C.F. Kaminski, P. St George-Hyslop, ALS/FTD mutation-induced phase transition of FUS liquid droplets and reversible hydrogels into irreversible hydrogels impairs RNP granule function, Neuron 88 (4) (2015) 678–690.
[35] A. Patel, H.O. Lee, L. Jawerth, S. Maharana, M. Jahnel, M.Y. Hein, S. Stoynov, J. Mahamid, S. Saha, T.M. Franzmann, A. Pozniakovski, I. Poser, N. Maghelli, L.A. Royer, M. Weigert, E.W. Myers, S. Grill, D. Drechsel, A.A. Hyman, S. Alberti, A liquid-to-solid phase transition of the ALS protein FUS accelerated by disease mutation, Cell 162 (5) (2015) 1066–1077.
[36] L.A. Strawn, T. Shen, N. Shulga, D.S. Goldfarb, S.R. Wente, Minimal nuclear pore complexes define FG repeat domains essential for transport, Nat. Cell Biol. 6 (3) (2004) 197–206.